Applied Physics Letters PERSPECTIVE pubs.aip.org/aip/apl

A look at the future of perovskite detectors

Cite as: Appl. Phys. Lett. **125**, 090501 (2024); doi: 10.1063/5.0228001
Submitted: 11 July 2024 · Accepted: 14 August 2024 ·
Published Online: 29 August 2024

A. Rogalski[a]

AFFILIATIONS

Institute of Applied Physics, Military University of Technology, 2 Kaliskiego St., 00-908 Warsaw, Poland

[a]Author to whom correspondence should be addressed: antoni.rogalski@wat.edu.pl

ABSTRACT

The perovskite materials have been broadly incorporated into optoelectronic devices due to a number of advantages such as high absorption coefficient, high carrier mobility, long carrier diffusion length, shallow defect levels, and high crystal quality. The rapid technological progress of perovskite devices is related to their relatively simple fabrication process, low production cost, and high efficiency.

This article first briefly introduces the basic physical properties of perovskite materials [mainly metal halide perovskites (MHPs)], which have a decisive impact on the performance of photodetectors. The most important parameters of perovskite detectors, such as current responsivity, detectivity, and response time, were then evaluated in comparison with standard photodiodes available on the commercial market. The conclusions presented in this paper are based on an analysis of published data in the vast literature. Some papers report detectivity close to the physical limit defined by signal fluctuations and background radiation, which tends to indicate that they are overestimated. Large discrepancies are observed in the demonstrated current responsivity and detectivity values, which may be due to two reasons: immature device technology and erroneous parameter estimates. This paper also attempts to determine the importance of perovskite detectors in the global market in the near future.

Significant improvements have been made in the performance of perovskite photodetectors operating in the visible and near-infrared regions,[1,2] particularly those made from a subgroup of metal halide perovskites (MHPs). Their development is mainly triggered by the progressive evolution of the solid-state perovskite considered as a robust candidate for next-generation solar cells. The utmost detectivity values for perovskite detectors are 3–4 orders of magnitude higher than commercially available standard visible photodiodes. However, large discrepancies are observed in the demonstrated current responsivity and detectivity values.

In this paper, we first present a brief summary of the fundamental physical properties of perovskite materials with decisive influence on photodetector performance, such as crystalline quality, absorption coefficient, carrier mobility, and carrier diffusion length. The most important parameters of perovskite detectors, such as current responsivity, detectivity, and response time, were then analyzed when confronted with standard photodiodes available on the commercial market. It has been shown that the record performance of perovskite detector is overestimated. The third/final part of the paper articulates the advantages and disadvantages of perovskite photodetectors, which will decisively determine their future place in the broad family of visible and near-infrared detector ranges.

Among the various types of perovskite materials, metal halide perovskites (MHPs) are emerging as a rising star in the field of optoelectronics. This subgroup of the perovskite family is characterized by nearly cubic structure with crystal unit cell given by the ABX_3 formula, where cation A can stabilize octahedra $[BX_6]^{4-}$, formed with cation B and halide X (Cl^-, Br^-, and I^-)—see Fig. 1(a). In terms of the photoelectrical conversion properties, the proper cations for metal halide perovskites are limited. Organic molecules, such as $CH_3NH_3^+$ (MA—methylammonium) and $CH(CH_2)_2^+$ (FA—formamidinium), and inorganic cations, such as Rb^+ and Cs^+, are used as monovalent A cations, while bivalent transition metal ions Mn^{2+}, Pb^{2+}, Sn^{2+}, and Ge^{2+} are implemented as B cations. The bivalent Pb ion is generally the optimal selection for B cations despite their Pb toxicity to the human body and environment. Elements such as Sn, Ge, Bi, and Cu have been implemented to replace Pb, but at the current stage of technology, the performance of perovskite optoelectronic devices using them is lower than those containing Pb.

By changing the elemental species in the perovskite materials, the optical and electrical properties and stability of perovskites can be significantly changed. The crystal structure of perovskites is sensitive to the ionic radius of the A-site cations because of the limitation of the octahedral $[BX_6]^{4-}$ framework. To study the stability of perovskites, Goldschmidt proposed the tolerance factor t and the octahedral factor μ.[3] The tolerance factor $t = (r_A + r_X)/\sqrt{2}(r_B + r_X)$ indicates the state of distortion and the octahedral factor is determined by the ratio of

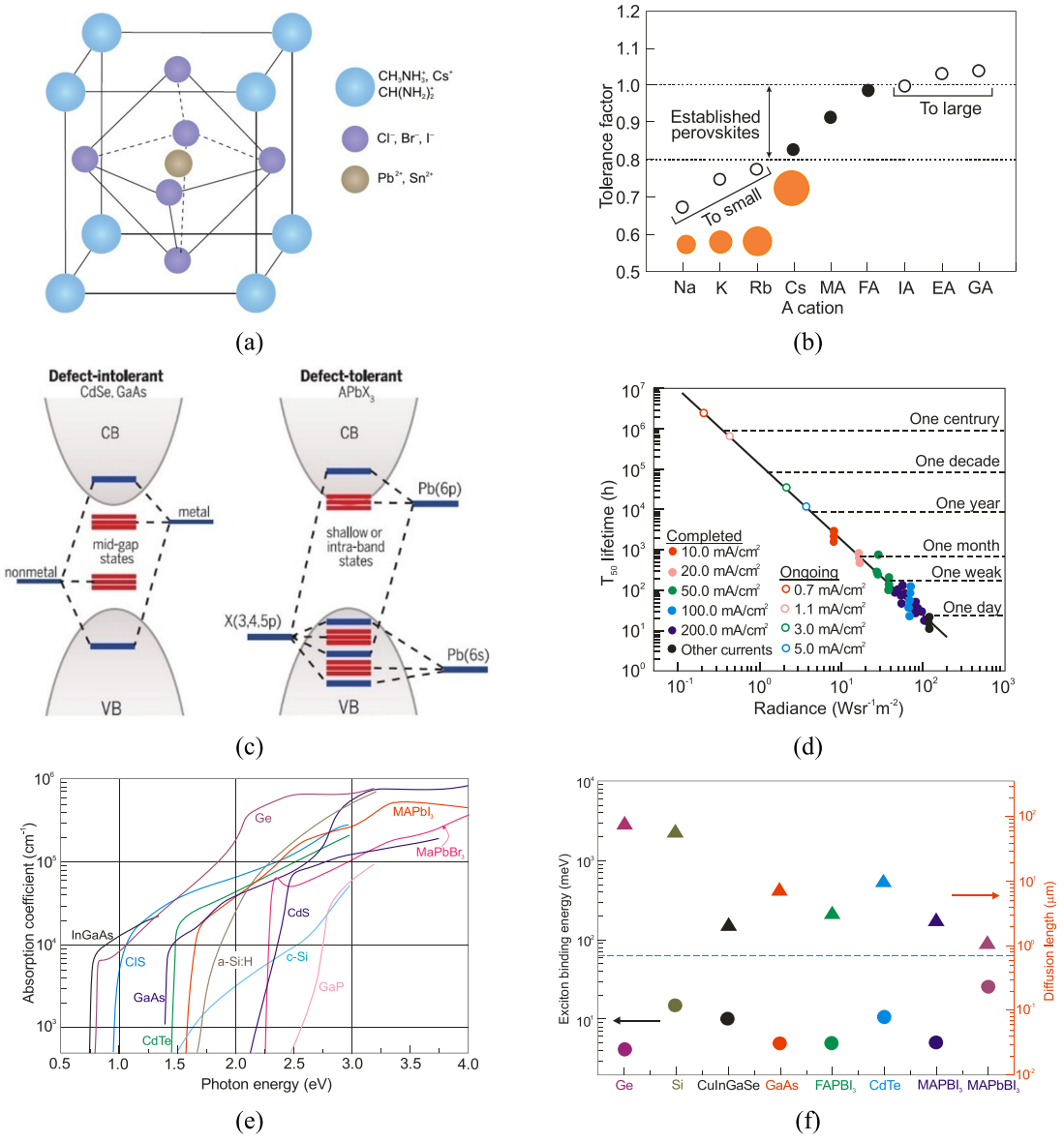

FIG. 1. Properties of perovskite materials: (a) the bulk perovskite structures with formula ABX_3 where A corresponds to the MA, FA, Cs^+ cations, B represents Pb_2^+ and Sn_2^+ metal cations, and X stands for Cl^-, Br^-, and I halogen anions; (b) tolerance factor of $APbI_3$ perovskites with various cations in the A-site (adapted after Ref. 4); (c) schematic of the electronic band structure of typical defect-intolerant semiconductors (e.g., CdSe, GaAs, and InP) (left) and defect-tolerant halide perovskite (e.g., $APbX_3$) (right) (Reprinted with permission from Kovalenko *et al.*, Science **358**, 745–750 (2017). Copyright 2017 American Association for the Advancement of Science[5]); (d) the T_{50} lifetimes as a function of initial radiance (data points marked by the solid dots are from completed T_{50} measurements, the open circles are the extrapolated T_{50} lifetimes for the ongoing measurements at medium and low current densities, which are expected to finish after longer times) (Reprinted with permission from Guo *et al.*, Nat. Photonics **16**, 637–643 (2022). Copyright 2022 Nature Research journals[8]); (e) absorption coefficient and (f) binding energy and diffusion length for selected semiconductor and perovskite materials (adapted after Ref. 10).

$\mu = r_A/r_X$. Here, r_A, r_B, and r_X are the ionic radii of the A-, B-, and X-site cations, respectively. In general, stable perovskites with ideal cubic structures can be obtained for $0.9 < t < 1.10$, while tetragonal and orthorhombic structures are formed for $0.81 < t < 0.9$. Figure 1(b) summarizes the changes in the tolerance factors according to the various cations in the A-site.[4] A-site cations such as Cs^+, $CH_3NH_3^+$ (MA), $HC(NH_2)_2^+$ (FA) can yield stable perovskite materials. Instead, smaller ones (Na^+, Ka^+, and Rb^+) can deform/destroy the crystal structure. From the other side, organic cations [e.g., imidazolium (IA^+), ethylamine (EA^+), and guanidinium (GA^+)] with larger ionic radii prompt the growth of octahedral $[BX_6]^{4-}$ along the in-plane direction and cannot enter the octahedral gap.

Unlike conventional semiconductor materials, in which defects act as trap states located between the bottom of the conduction band (CB) and the top of the valence band (VB), the orbitals in perovskites are located inside or near the edges of the VB and CB bands—see Fig. 1(c).[5] This makes perovskites highly tolerant to defects. These defects do not act as trap states and therefore their effects are mild on the electronic and optical properties of the devices. This benefit is particularly evident in flexible photodetectors, which must withstand various mechanical deformations.

The critical problem of lead perovskite with organic cations that needs to be solved is that of thermal and structural instability caused by ion migration and trapped charges.[6] The bulk MA-based perovskites were found to be instable due to the fairly hazardous MA cations.[7] Generally, the ionic nature perovskites are not that stable as inorganics. In humid environment, they can drastically change the crystalline structure and composition, causing permanent material damage. Effective housing is needed to fully protect the device while long-term stability under extremely harsh operating conditions also remains an issue.

More recently, a collaboration of several Chinese research groups made an important breakthrough in the field of perovskite NIR light-emitting diodes—LEDs (~800 nm).[8] They have discovered that by using a dipolar molecular stabilizer [sulfobetaine 10 (SFB10)], it is possible to produce efficient and stable perovskite LEDs with much longer lifetimes to meet the requirements of commercial applications [see Fig. 1(d)]. The key to this stability is the introduction of a stabilizer that interacts with cations and anions at the perovskite grain boundaries slowing down the migration of ions in the electric field. The estimated T_{50} lifetime is 32 675 h (3.7 years) at an initial radiance of 2.1 W/srm2 (3.2 mA/cm^2). However, this optimistic result has not been confirmed by other scientific groups.[9]

By changing the elemental species in the perovskite materials, the optoelectronic properties of perovskites can be significantly changed. The significant optoelectronic properties (absorption coefficient, binding energy and diffusion length) of perovskite materials compared to the standard semiconductors are presented in Figs. 1(e) and 1(f).[10]

Table I summarizes the unique properties of perovskite materials.[11–13] The high efficiency of photovoltaic devices is credited to the high electron mobility (up to 200 cm^2/V s) along with a long diffusion length (>1 μm). Their absorption coefficients are reported at the level between 10^4 and 10^5 cm^{-1}, caused by s–p antibonding coupling. Another beneficial property is a low exciton binding energy <10 meV allowing the excited carriers to migrate as free carriers.[11]

TABLE I. The optical and electronic parameters of MHP materials.

Parameter	Value
Energy bandgap	1.5–2.5 eV
Absorption coefficient	10^4–10^5 cm^{-1}
Exciton binding energy	<10 meV
Crystallization energy barrier	56.6–97.3 kJ/mol
PL quantum efficiency	70%
Charge carrier lifetime	Greater than 300 ns
Relative permittivity	3
Carrier mobility	≈50–200 cm^2/Vs
Exciton	Wannier type exciton
Trap-state density	10^{10} cm^{-3} (single crystals) 10^{15}–10^{17} cm^{-3} (polycrystals)

MHP materials are the most advantages of the crystalline states and display better optical and electrical capabilities than polycrystalline films and microcrystals. This is due to structural advantages such as free grain boundaries, an ordered long-range crystal structure, and its high orientation resulting in greater stability.

There have been many reports on perovskite-based photodetectors. For this reason, this article is limited to describing the most important parameters that will affect the further development of perovskite photodetectors in the future.

The photodetectors reach the most favorable conditions when the intrinsic detector noise is low in comparison to the photon noise.[14,15] The radiation incident on the detector is built of two parts coming from target and background. There are two detector's fundamental performance maximum value: the signal fluctuation limit (SFL) and the background fluctuation limit, also known as the BLIP (background limited infrared photodetector).

Figure 2 presents the ultimate detectivities reported for selected photon detectors within the 0.2–2 μm wavelength range for 300 K scene temperature and 2π field of view (FOV). As shown, the SFL and BLIP curves crossing is located ~1.2 μm and below <1.2 μm, where the device operates under SFL, the D^* wavelength dependence is weak; while for >1.2 μm BLIP dominates and D^* dependence is strong resulting from intense increase in the background radiation influence at the edge of the spectral distribution at 300 K.

The experimental data highlighted in Fig. 2 are for standard photodetectors available on the commercial market and the rest of the data are limited only for high-performance perovskite photodetectors

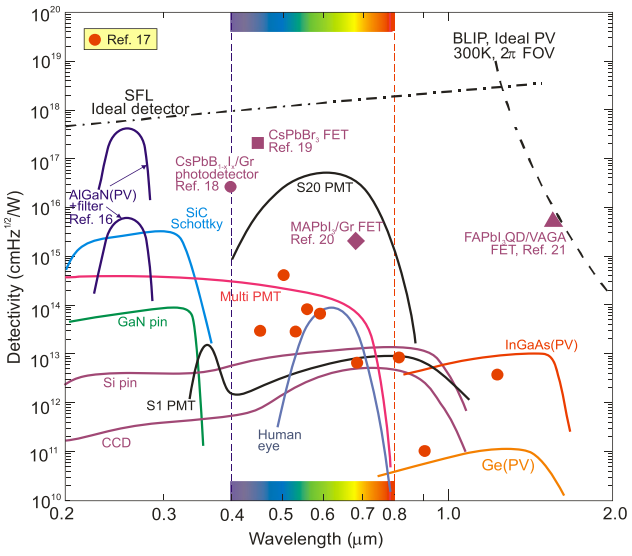

FIG. 2. Comparison of room-temperature detectivities of perovskite photodetectors[17–21] with standard commercially detectors available on the global market (AlGaN, Si, Ge, InGaAs photodiodes, and PMTs) in the wavelength range 0.2–2 μm. The ultimate SFL and BLIP limits are also shown. PV—photovoltaic detector, PMT—photomultiplier tube, FET—field effect transistor. The detectivity values of perovskite photodetectors marked in magenta are probably overestimated.

published in the literature. In terms of standard detectors, AlGaN photodiodes exhibit the highest D^* at 260 nm close to the SFL Limit. However, to reach such a high D^*, it is essential to use filters to suppress solar-irradiance leakage.[16] The highest detectivity values for perovskite photodetectors,[17–21] highlighted in magenta, are located above those of standard photodetectors. In addition, the papers signaling the highest detectivities do not indicate that optical filters were used in the detectors whose characteristics were measured. It is expected that the detectivity values of perovskite photodetectors marked in magenta are overestimated.

A proper photodetector characterization requires at least some experimental evaluation of noise itself in the actual device under test. In order to estimate D-star (D^*), the contribution of the different types of noise should be taken into account: shot, generation–recombination (g-r), photon, thermal, and $1/f$ noises. However, many reports do not consider the photogain effect's influence on the shot and gr noises mainly for room-temperature devices exhibiting low response rate caused by long carrier lifetimes (typical for hybrid photodetectors—phototransistors). Assuming incorrect expression for the shot noise ($I_{sh} = \sqrt{2qI\Delta f}$ rather than of $I_{sh} = \sqrt{2qgI\Delta f}$) causes false improvement (record-breaking performances) in the signal-to-noise ratio (SNR) by a factor of $\sqrt{g}$ in relation to the SNR at the detector input. A similar dependence on $\sqrt{g}$ occurs for generation–recombination noise since $I_{g\text{-}r} = \sqrt{4qI_dg\Delta f/(1+\omega^2\tau^2)}$ (the g-r noise is frequency-related, ω). The shot/g-r noises' estimate error increases for higher g and is principally significant for photodetectors exhibiting high internal gain. For further discussion on this topic, see below.

Additionally, researchers should report details of their experimental values (measured current, voltages, and their variances) and detailed experimental and numerical procedures for the calculation of derived quantities (e.g., the detectivity) so that an informed comparison between reports can be made. Moreover, non-linearity in light response and in the electrical conduction is not uncommon in perovskites as well as many other materials (see, e.g., Ref. 22).

There are several reports stressing the cases where photodetector performance is overestimated by wrong characterization procedures due to (1) erroneous noise estimates, (2) miscalculations of the device's active area and light power density, and (3) conflicting bandwidths adopted for the measured noise and sensitivity.[23–26] For this reason, perovskite photodetectors require appropriate characterization procedures consistent with those used for typical bulk photodetectors.

Over the past six years, many papers have been published demonstrating the high performance of perovskite photodetectors. In the following analysis, we will try to sort out the published performance of photodetectors and provide an analysis explaining the large discrepancies in their values.

At first, to benchmark the presented results, Fig. 3 collects the performance (current responsivity, R_i, and detectivity, D^*) of different types of perovskite-based hybrid photodetectors (FET phototransistors) and compares the values with standard visible photodiodes. A detailed description of photodetector parameters presented in Figs. 3–5 is given in Table II. The utmost D^* for perovskite detectors are 3–4 orders of magnitude higher than commercially available crystalline Si photodiodes. Large discrepancies are observed in the demonstrated current responsivity and detectivity values, which may be due to two reasons: immature device technology and erroneous detectivity estimates.

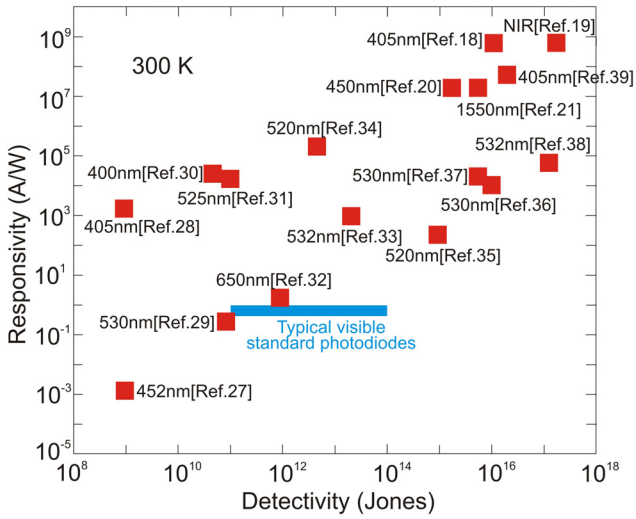

FIG. 3. Comparison of R_i and D^* for hybrid perovskite-based photodetectors at 300 K. The data are collected from the literature as noted in the figure.[19–21,27–39] For comparison purposes, the range of typical performance for visible photodiodes is also marked.

Further insight in detectors performance gives Fig. 4 where is shown the dependence of detectivity on and gain collected from literature for high quantity perovskite-based photodetector structures. This figure also highlights theoretical predictions for the SFL limit for the wavelength range of 400–800 nm. The dominant areas of D^*/g for each type of photodetector—photodiodes, photoconductors, and FET phototransistors—are also marked. The highest D^*-values, including partially unrealistic ones (close to SFL limits), are marked for FET phototransistors with large photogating effect (up to above 10^9).

It is believed that the main reason for the overestimation of detectivity values (close to the SFL limit) is the incorrect/(or lack of) consideration of the internal gain in shot noise and generation–recombination noise values. The data from Ref. 21 and highlighted in Figs. 1–3 are for the NIR FET/FAPbI$_3$QD/VAGA perovskite photodetector operating at 1550 nm and are closed to the BLIP limit.

Perovskite-based photodetectors, primarily hybrid (FET) devices, allow to increase responsivity; however, the majority of those devices exhibit a limited linear dynamic range (LDR) caused by the charge relaxation time quickly saturating the available photoexcitation states, leading to responsivity drop vs incident optical power.[40] The significance of that effect is fact that high-sensitivity detectors exhibit a low response rate, observed over a wide spectral range and confirmed by the experimental data shown in Fig. 5. Response times up to a few seconds were reported for photodetectors with high gain (above 10^9). This is a challenge and trade-off in reaching both high photoresponsivity and a fast response at once.

In summary, perovskite materials have developed as perspective ones in last decade what is directly related to the excellent processability and improved carrier transport capabilities similar to the typical semiconductors allowing them to be easily implemented into numerous device's applications to include: thin films solar cells, photodetectors, light-emitting diodes, lasers, transistors, etc.

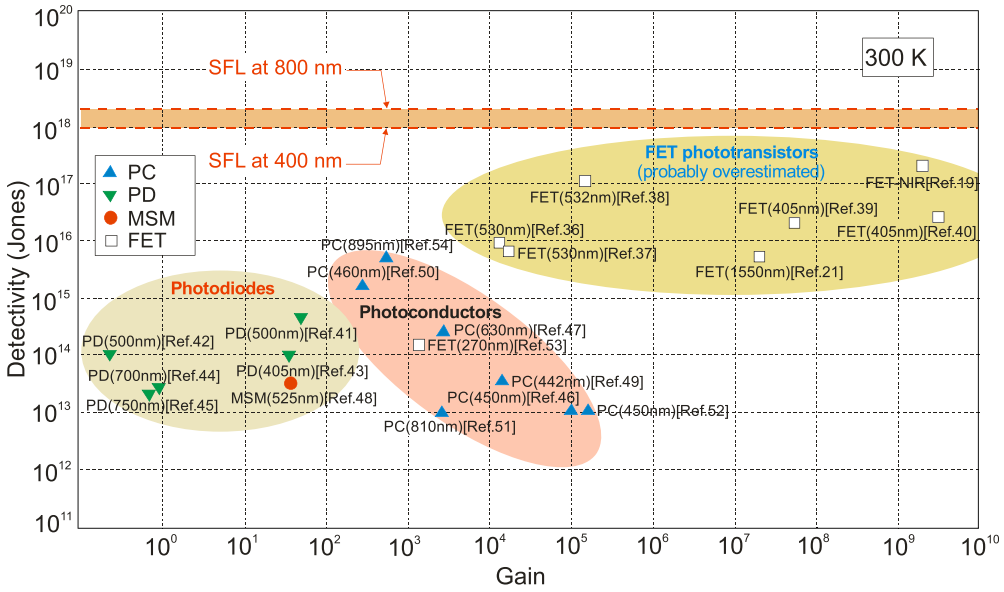

FIG. 4. Plot of the dependence of detectivity on gain for different types of perovskite-based photodetectors at room temperature. The data are collected from the literature as noted in the figure[19,21,36–54]. Theoretical predictions for SFL limit for the wavelength range of 400–800 nm are also highlighted. Designations: PC—photoconductor, PD—photodiode, FET—field effect transistor, and MSM—metal–semiconductor–metal.

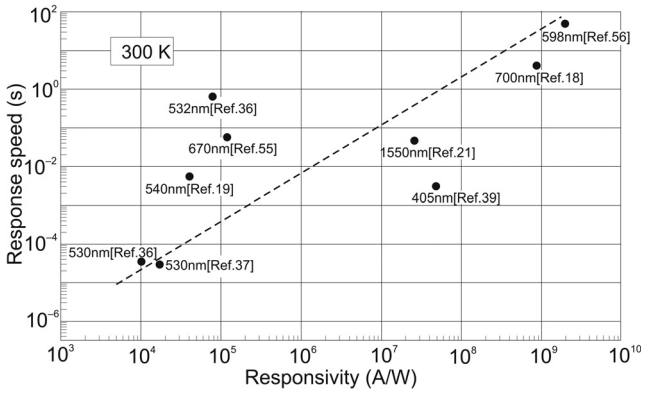

FIG. 5. The current responsivity dependence on the response time for perovskite-based hybrid photodetectors at 300 K. Experimental data were taken from selected papers as marked.[18,19,21,36,37,39,56]

The most important features of perovskites are articulated as follows:

- A wide variety of perovskites have a direct and tunable energy gap controlled by mixing. Their electronic properties (doping) can also be controlled by the composition. The fabrication methods are relatively simple; however, their physical properties are affected by other factors, e.g., morphology, grain size, crystallinity, and processing history.
- Perovskites are promising materials for future applications, including traditional optoelectronic devices. Their triggered progressive development of the next-generation solar cells has strong influence on photodetector development. Up to now, however, most of the perovskite materials and devices have been fabricated on the laboratory scale.
- The performance of perovskite-based photodetectors has been found to be overestimated in many cases due to (1) erroneous noise estimates, (2) miscalculations of the device's active area and light power density, and (3) conflicting bandwidths adopted for the measured noise and sensitivity.
- Several methods including the use of electron trap layers and photogate effect with fast transfer channel can be implemented to improve sensitivity, but the limitation of carrier mobility and response time limit practical applications (trade-off between sensitivity and response time).
- In terms of application, several issues remain unresolved: The ionic nature perovskites are not as stable as inorganic ones and effective housing is needed to fully protect the device.
- Toxicity is another issue. So far, lead-based perovskites have been the materials exhibiting the best performance. Lead-free perovskites are gradually being introduced; however, their long-term stability issues are serious drawbacks that hinder the potential progression of these materials.[57]

To summarize the results analyzed and discussed in this paper, the opportunities for perovskite device technology are manifold. Their low-cost processability, abundance of starting materials, and excellent (compositional) flexibility provide a distinct advantage over III–V semiconductors. The biggest drawback of perovskites appears to be their instability. So far, the suggestion in Ref. 8 that perovskite devices are not "genetically defective" in terms of stability has not been confirmed by most research groups. Despite this, commercialization of perovskite-based devices appears to be a matter of time.[9,58,59] Recently,

TABLE II. Perovskite photodetectors—device/materials/performance.

Device/materials	Morphology	Spectral region (nm)	R (A/W) @ V_{bias} (V), [λ (nm), P (W/cm^2)]	D^*[a] (Jones) @ V_{bias} (V) [λ (nm), P(mW/cm^2)]	Rise time/ fall time	Reference
Photodiodes						
PD/ZnO-$CH_3NH_3PbI_3$-MoO_3	NC	200–800	24.3 @ 0 (500)	3.56×10^{14} @ 0 (500)	0.7/0.6 s	41
PD/GaN-$CsPbBr_3$-ZnO	NC	300–650	0.090 @ 0 (550)	1.03×10^{14} @ 0 (550)	100/140 ms	42
PD/$CsPbBr_3$	QDs	4	10.1 @ -1.5 (405)	9.35×10^{13} 0 (405)	⋯	43
PD/FTO-CdS-perovskite-Spiro-OMeTAD-Ag	NC	350–800	0.48 @ 0 (550)	2.1×10^{13} @ 0 (550)	0.54/2.21 ms	44
PD/FTO-bl-TiO_2-mp-TiO_2-perovskite/PTAA/Au	NC	350–750	0.192	8.8×10^{12}	53/38 μs	45
PD/$CH_3NH_3PbBr_3$	SC	350–550	20 @ 4 (500)	6×10^{13} @ 0 (525)	≈40 ms	48
Photoconductors						
PC/$CsPbBr_3$	NC	450	6.4×10^4@ 3	≈10^{13}	0.5/1.6 ms	46
PC/α-$CsPbI_3$	NW	630	1294	2.6×10^{14}	0.85/0.78 ms,	47
PC/$MAPbBr_3$	SC	3380–600	>4000 @ 5 (525)	$>3 \times 10^{13}$	∼25/25 μs	49
$(PEA)_2PbI_4$ 0.6 μm thick 2D plates	NC	460	98.2 @ 4	1.6×10^{15}	64/52 μs	50
PC/$MAPbI_3$	SC	400–850	1640 @ 1 (810)	≈10^{13}	30/20 μs	51
PC/$CH_3NH_3PbI_3$	SC0	400–900	568 @ (895)	5.5×10^{15}	0.22/0.16 s	54
Field effect phototransistors						
FET/$Sr_2Nb_3O_{10}$	NC	250–500	1214 @ (270)	1.4×10^{14}@ 1 (270)		53
FET/$CsPbBr_{3-x}I_x$-graphene	NC	400-700	8.2×10^8 @ (405, 0.07 m)	∼10^{16} @ (405, 0.07)	0.81/3.65 s	18
FET/$FAPbI_3$QD/VAGA	QD	1550	2.2×10^7	5.6×10^{15}	46/46 ms	21
FET/CNT/$CsPbBr_3$QD	QD	405	5.1×10^7 @ (405, 10 n)	2×10^{16}	3 ms	39
FET/PDOT:PSS/ $CH_3NH_3PbI_{3-x}Cl_x$		598	1.9×10^9 @ ($V_D = 0.5$ V)	1.4×10^{14}	57.5 s	56
FET$(ThMA)_2(MA)_{n-1}Pb_nI_{3n+1}$ (n = 3)	NW	530	1.1×10^4 @ 5	9.1×10^{15} @ 5	36.2–31.5 μs	36
FET/$(BA)_2(MA)_{n-1}Pb_nI3_{n+1}$ (n = 4)	NW	530	1.5×10^4 @ 5	7×10^{15} @ 5	27.6–24.5 μs	37
FET/s-CNT/$(PEA)_2SnI_4$	NC	532	6.3×10^4 ($V_{DS} = 10$ V, $V_G = -40$ V)	1.12×10^{17}	825/440 ms	38
FET/$FAPbBr_3$/-graphene	QD	650	1.15×10^5	⋯	58/60 ms	55

[a]PD—photodiode, PC—photoconductor, FET—field effect transistor, PF—polycrystalline, SC—single crystals, NW—nanowires, NC—nanocrystals, QD—quantum dots, R—responsivity, D^*—detectivity, and P—intensity.

Ahn and Hu[9] have discussed advances on the strategies to slow down the degradation during operation for practical use of perovskite-based devices. Thus, further expansion of the perovskite materials family into optoelectronic applications is perceived to be still ahead.

This paper was supported by the Polish National Science Center within Project No. UMO-2023/48/Q/ST7/00144.

AUTHOR DECLARATIONS

Conflict of Interest

The authors has no conflicts to disclose.

Author Contributions

Antoni Rogalski: Conceptualization (equal); Formal analysis (equal); Investigation (equal); Methodology (equal); Resources (equal); Software (equal); Supervision (equal); Validation (equal); Visualization (equal); Writing – original draft (equal); Writing – review & editing (equal).

DATA AVAILABILITY

The data that support the findings of this study are available from the corresponding author upon reasonable request.

REFERENCES

[1]*Perovskite Photovoltaics and Optoelectronics. From Fundamentals to Advanced Applications*, edited by T. Miyasaka (Wiley-VCH GmbH, Weinheim, 2022).

[2]*Perovskite Materials and Devices*, edited by L. Ding (Wiley-VCH GmbH, Weinheim, 2022).

[3]V. M. Goldschmidt, Naturwissenschaften **14**(21), 477–485 (1926).
[4]L. N. Quan, B. P. Rand, R. H. Friend, S. G. Mhaisalkar, T.-W. Lee, and E. H. Sargent, Chem. Rev. **119**(12), 7444–7477 (2019).
[5]M. V. Kovalenko, L. Protesescu, and M. I. Bodnarchuk, Science **358**, 745–750 (2017).
[6]Y. Wang, M.-L. Gao, J.-L. Wu, and X.-W. Zhang, Chin. Phys. B **28**(1), 018502 (2019).
[7]B. Conings, J. Drijkoningen, N. Gauquelin, A. Babayigit, J. D'Haen, L. D'Olieslaeger, A. Ethirajan, J. Verbeeck, J. Manca, E. Mosconi, F. De Angelis, and H.-G. Boyen, Adv. Energy Mater. **5**(15), 1500477 (2015).
[8]B. Guo, R. Lai, S. Jiang, L. Zhou, Z. Ren, Y. Lian, P. Li, X. Cao, S. Xing, Y. Wang, W. Li, C. Zou, M. Chen, Z. Hong, C. Li, B. Zhao, and D. Di, Nat. Photonics **16**, 637–643 (2022).
[9]N. Ahn and M. Cho, Adv. Sci. **11**, 2306110 (2024).
[10]A. Rajagopal, K. Yao, and A. K.-Y. Jen, Adv. Mater. **30**, 1800455 (2018).
[11]A. Miyata, A. Mitioglu, P. Plochocka, O. Portugall, J. T.-W. Wang, S. D. Stranks, H. Snaith, and R. Nicholas, Nat. Phys. **11**, 582–587 (2015).
[12]L. M. Herz, ACS Energy Lett. **2**, 1539–1548 (2017).
[13]P. Roy, A. Ghosh, F. Barclay, A. Khare, and E. Cuce, Coatings **12**, 108 (2022).
[14]P. W. Kruse, "The photon detection process," in *Optical and Infrared Detectors*, edited by R. J. Keyes (Springer, Berlin, 1977), pp. 5–69.
[15]E. L. Dereniak and G. D. Boremen, *Infrared Detectors and Systems* (Wiley, New York, 1996).
[16]X. Li, C. Zhu, X. Zhu, Z. Xu, X. Zhuang, X. Ji, and F. Yan, Appl. Phys. Lett. **103**, 171110 (2013).
[17]H. Wang and D. H. Kim, Chem. Soc. Rev. **46**, 5204–5236 (2017).
[18]D. H. Kwak, D. H. Lim, H. S. Ra, P. Ramasamy, and J. S. Lee, RSC Adv. **6**, 65252–65256 (2016).
[19]Y. Yu, Y. Zhang, L. Jin, Z. Chen, Y. Li, Q. Li, M. Cao, Y. Che, and J. Yao, Proc. SPIE **10914**, 1091419 (2019).
[20]P.-H. Chang, S.-Y. Liu1, Y.-B. Lan, Y.-C. Tsai, X.-Q. You, C.-S. Li, K.-Y. Huang, A.-S. Chou, T.-C. Cheng, J.-K. Wang, and C.-I. Wu, Sci. Rep. **7**, 46281 (2017).
[21]X. Feng, Z. He, W. Zhu, M. Zhao, Z. Liu, S. Yang, S. Tang, Q. Guo, Z. Jin, D. Chen, G. Ding, and G. Wang, J. Mater. Chem. C **9**, 609–619 (2021).
[22]Y. Fang, A. Armin, P. Meredith, and J. Huang, Nat. Photonics **13**(1), 1–4 (2019).
[23]S. Bianconi, L. J. Lauhon, and H. Mohseni, Nat. Photonics **15**, 714 (2021).
[24]A. Rogalski, Nat. Nanotechnol. **17**, 217–219 (2022).
[25]A. Rogalski, IEEE Electron Device Lett. **44**, 805–808 (2023).
[26]F. Wang, T. Zhang, R. Xie, Z. Wang, and W. Hu, Nat. Commun. **14**, 2224 (2023).
[27]Z. Chen, Z. Kang, C. Rao, Y. Cheng, N. Liu, Z. Zhang, L. Li, and Y. Gao, Adv. Electron. Mater. **5**, 1900168 (2019).
[28]Y. Che, Y. X. Cao, Y. Zhang, and J. Yao, Opt. Mater. **100**, 109664 (2020).
[29]J. Li, S. Yuan, G. Tang, G. Li, D. Liu, J. Li, X. Hu, Y. Liu, J. Li, Z. Yang, S. F. Liu, Z. Liu, F. Gao, and F. Yan, ACS Appl. Mater. Interfaces **9**, 42779–42787 (2017).
[30]J. Chen, Q. Jing, F. Xu, Z. Lu, and Y. Lu, Optica **4**, 835–838 (2017).
[31]A. Surendran, X. Yu, R. Begum, Y. Tao, Q. J. Wang, and W. L. Leong, ACS Appl. Mater. Interfaces **11**, 27064–27072 (2019).
[32]M. Zhang, F. Zhang, Y. Wang, L. Zhu, Y. Hu, Z. Lou, Y. Hou, and F. Teng, Sci. Rep. **8**, 11157 (2018).
[33]Y. Zou, T. Zou, C. Zhao, B. Wang, J. Xing, Z. Yu, J. Cheng, W. Xin, J. Yang, W. Yu, H. Dong, and C. Guo, Small **16**, 2000733 (2020).
[34]A. A. Bessonov, M. Allen, Y. Liu, S. Malik, J. Bottomley, A. Rushton, I. Medina-Salazar, M. Voutilainen, S. Kallioinen, A. Colli, C. Bower, P. Andrew, and T. Ryhänen, ACS Nano **11**, 5547–5557 (2017).
[35]Y. Lee, J. Kwon, E. Hwang, C. H. Ra, W. J. Yoo, J. H. Ahn, J. H. Park, and J. H. Cho, Adv. Mater. **27**, 41–46 (2015).
[36]Y. Zhao, Y. Qiu, H. Gao, J. Feng, G. Chen, L. Jiang, and Y. Wu, Adv. Mater. **32**, e1905298 (2020).
[37]J. Feng, C. Gong, H. Gao, W. Wen, Y. Gong, X. Jiang, B. Zhang, Y. Wu, Y. Wu, H. Fu, L. Jiang, and X. Zhang, Nat. Electron. **1**, 404 (2018).
[38]H. Zhu, A. Liu, H. L. Luque, H. Sun, D. Ji, and Y. Y. Noh, ACS Nano **13**, 3971–3981 (2019).
[39]Q.-B. Zhu, B. Li, D.-D. Yang, C. Liu, S. Feng, M.-L. Chen, Y. Sun, Y.-N. Tian, X. Su, X.-M. Wang, S. Qiu, Q.-W. Li, X.-M. Li, H.-B. Zeng, H.-M. Cheng, and D.-M. Sun, Nat. Commun. **12**, 1798 (2021).
[40]G. Abiram, M. Thanihaichelvan, P. Ravirajan, and D. Velauthpillai, Nanomater. **12**, 2396 (2022).
[41]J. Yu, X. Chen, Y. Wang, H. Zhou, M. Xue, Y. Xu, Z. Li, C. Ye, J. Zhang, P. A. van Aken, P. D. Lund, and H. Wang, J. Mater. Chem. C **4**, 7302–7308 (2016).
[42]C. Tian, F. Wang, Y. Wang, Z. Yang, X. Chen, X. Mei, H. Liu, and D. Zhao, ACS Appl. Mater. Interfaces **11**, 15804–15812 (2019).
[43]K. Shen, H. Xu, X. Li, J. Guo, S. Sathasivam, M. Wang, A. Ren, K. L. Choy, I. P. Parkin, Z. Guo, and J. Wu, Adv. Mater. **32**, e2000004 (2020).
[44]F. Cao, L. Meng, M. Wang, W. Tian, and L. Li, Adv. Mater. **31**, e1806725 (2019).
[45]D. S. Lee, J. H. Heo, J. K. Park, B. W. Kim, H. J. Lee, Y. M. Song, and S. H. Im, ACS Appl. Mater. Interfaces **13**, 16775–16775 (2021).
[46]B. Yang, F. Zhang, J. Chen, S. Yang, X. Xia, T. Pullerits, W. Deng, and K. Han, Adv. Mater. **29**, 1703758 (2017).
[47]G. Chen, J. Feng, H. Gao, Y. Zhao, Y. Pi, X. Jiang, Y. Wu, and L. Jiang, Adv. Funct. Mater. **29**, 1808741 (2019).
[48]Y. Liu, Y. Zhang, K. Zhao, Z. Yang, J. Feng, X. Zhang, K. Wang, L. Meng, H. Ye, M. Liu, and S. F. Liu, Adv. Mater. **30**, 1707314 (2018).
[49]Y. Chen, G. Chen, Z. Zhou, X. Li, P. Ma, L. Li, W. Yin, H. Zeng, and G. Zou, Adv. Funct. Mater. **31**, 2101966 (2021).
[50]Y. Liu, Y. Zhang, Z. Yang, H. Ye, J. Feng, Z. Xu, X. Zhang, R. Munir, J. Liu, P. Zuo, Q. Li, M. Hu, L. Meng, K. Wang, D.-M. Smilgies, G. Zhao, H. Xu, Z. Yang, A. Amassian, J. Li, K. Zhao, and S. Liu, Nat. Commun. **9**, 5302 (2018).
[51]M. I. Saidaminov, M. A. Haque, M. Savoie, A. L. Abdelhady, N. Cho, I. Dursun, U. Buttner, E. Alarousu, T. Wu, and O. M. Bakr, Adv. Mater. **28**, 8144–8149 (2016).
[52]X. Li, D. J. Chen, Y. Wang, F. Cao, Y. Wei, Y. Wu, L. Wang, Y. Zhu, Z. Sun, J. Ji, Y. Shen, H. Sun, and H. Zeng, ACS Nano **11**, 2015–2023 (2015).
[53]S. Li, Y. Zhang, W. Yang, H. Liu, and X. Fang, Adv. Mater. **32**, e1905443 (2020).
[54]J. Xin, Q. Wang Q, J. Li, K. Wang, W. Deng, J. Jin, M. Peng, M. Fang, J. Qu, and H. Wang, J. Phys. D **53**, 414003 (2020).
[55]R. Pan, H. Li, J. Wang, X. Jin, Q. Li, Z. Wu, J. Gou, Y. Jiang, and Y. Song, Particle **35**, 1700304 (2018).
[56]C. Xie, P. You, Z. Liu, L. Li, and F. Yan, Light **6**, e17023 (2017).
[57]E. Aktas, N. Rajamanickam, J. Pascual, S. Hu, M. H. Aldamasy, D. Di Girolamo, W. Li, G. Nasti, E. Martínez-Ferrero, A. Wakamiya, E. Palomares, and A. Abate, Commun. Mater. **3**, 104 (2022).
[58]J. Y. Kim, J.-W. Lee, H. S. Jung, H. Shin, and N.-G. Par, Chem. Rev. **120**(15), 7867–7918 (2020).
[59]T.-H. Han, K. Y. Jang, Y. Dong, R. H. Friend, E. H. Sargent, and T.-W. Lee, Nat. Rev. Mater. **7**, 757–777 (2022).